FULL PAPER

The Importance of Fullerene Percolation in the Mixed Regions of Polymer–Fullerene Bulk Heterojunction Solar Cells

*Jonathan A. Bartelt, Zach M. Beiley, Eric T. Hoke, William R. Mateker, Jessica D. Douglas, Brian A. Collins, John R. Tumbleston, Kenneth R. Graham, Aram Amassian, Harald Ade, Jean M. J. Fréchet, Michael F. Toney, and Michael D. McGehee**

Most optimized donor-acceptor (D-A) polymer bulk heterojunction (BHJ) solar cells have active layers too thin to absorb greater than ~80% of incident photons with energies above the polymer's band gap. If the thickness of these devices could be increased without sacrificing internal quantum efficiency, the device power conversion efficiency (PCE) could be significantly enhanced. We examine the device characteristics of BHJ solar cells based on poly(di(2-ethylhexyloxy)benzo[1,2-*b*:4,5-*b*′]dithiophene-*co*-octylthieno[3,4-*c*]pyrrole-4,6-dione) (PBDTTPD) and [6,6]-phenyl-C_{61}-butyric acid methyl ester (PCBM) with 7.3% PCE and find that bimolecular recombination limits the active layer thickness of these devices. Thermal annealing does not mitigate these bimolecular recombination losses and drastically decreases the PCE of PBDTTPD BHJ solar cells. We characterize the morphology of these BHJs before and after thermal annealing and determine that thermal annealing drastically reduces the concentration of PCBM in the mixed regions, which consist of PCBM dispersed in the amorphous portions of PBDTTPD. Decreasing the concentration of PCBM may reduce the number of percolating electron transport pathways within these mixed regions and create morphological electron traps that enhance charge-carrier recombination and limit device quantum efficiency. These findings suggest that (i) the concentration of PCBM in the mixed regions of polymer BHJs must be above the PCBM percolation threshold in order to attain high solar cell internal quantum efficiency, and (ii) novel processing techniques, which improve polymer hole mobility while maintaining PCBM percolation within the mixed regions, should be developed in order to limit bimolecular recombination losses in optically thick devices and maximize the PCE of polymer BHJ solar cells.

1. Introduction

Polymer-based bulk heterojunction (BHJ) solar cells[1] consisting of electron-donating polymers and electron-accepting fullerene derivatives garner interest because they can be printed at low cost onto lightweight, flexible substrates. The certified power conversion efficiencies (PCEs) of single junction polymer BHJ solar cells are now approaching 9%[2,3] due to (i) the development of new low band gap donor-acceptor (D-A) polymers with broad absorption capabilities,[4,5] (ii) the development of polymers and fullerene derivatives with energy levels optimized for high open-circuit voltages (V_{OC}),[6,7] and (iii) the use of solvent additives to tailor BHJ morphology.[8,9] Despite these improvements, most optimized D-A polymer BHJ solar cells with PCE greater than 7% are too thin to absorb greater than ~80% of incident photons with energies above the polymer's band gap, substantially limiting potential photocurrent.[6,9–14] Unfortunately, D-A polymer BHJ solar cells with optically thick active layers generally have lower PCEs than their thin active layer counterparts, primarily due to lower fill factors (FFs).[15] In contrast, poly(3-hexylthiophene) (P3HT) BHJ solar

J. A. Bartelt, Z. M. Beiley, W. R. Mateker, Dr. K. R. Graham, Prof. M. D. McGehee
Department of Materials Science and Engineering
Stanford University
Stanford, CA 94305, USA
E-mail: mmcgehee@stanford.edu
Dr. E. T. Hoke
Department of Applied Physics
Stanford University
Stanford, CA 94305, USA
J. D. Douglas, Prof. J. M. J. Fréchet
Department of Chemistry,
University of California
Berkeley, CA 94720, USA
Dr. B. A. Collins, Dr. J. R. Tumbleston, Prof. H. Ade
Department of Physics
North Carolina State University
Raleigh, NC 27695, USA
Dr. K. R. Graham, Prof. A. Amassian, Prof. J. M. J. Fréchet
Division of Physical Sciences and Engineering
King Abdullah University of Science and Technology
Thuwal, 23955-6900, Saudi Arabia
Dr. M. F. Toney
Stanford Synchrotron Radiation Lightsource
SLAC National Accelerator Laboratory
Menlo Park, CA 94025, USA

DOI: 10.1002/aenm.201200637

cells are optimal with thick active layers and can absorb greater than 90% of incident photons with energies above P3HT's band gap while maintaining FFs near 0.70.[16] In optically thick P3HT BHJ devices, charge-carriers are efficiently extracted despite the fact that blending [6,6]-phenyl-C_{61}-butyric acid methyl ester (PCBM) with P3HT decreases the hole mobility in P3HT by up to three orders of magnitude.[16,17] These charge-carriers can be efficiently extracted because thermal and solvent annealing improve the hole mobility in P3HT BHJs to nearly that in pure P3HT.[16,17] D-A polymer BHJ solar cells, however, generally lose PCE when thermally annealed,[6,9–14] indicating that the as-cast morphology of these devices is essential for optimal performance. The reason for this difference between P3HT and D-A polymers is still not well understood.

Herein we examine the device characteristics and morphology of BHJ solar cells based on a D-A polymer, poly(di(2-ethylhexyloxy)benzo[1,2-*b*:4,5-*b*′]dithiophene-*co*-octylthieno[3,4-*c*]pyrrole-4,6-dione) (PBDTTPD),[18–20] (**Figure 1**a) and PCBM. Optimized PBDTTPD BHJ solar cells achieve 7.3% PCE with a V_{OC} up to ~0.95 V and an internal quantum efficiency (IQE) near 90%.[21] These devices, however, only absorb 60–80% of incident photons with energies above PBDTTPD's and PCBM's band gaps, and increasing the device active layer thickness decreases the PCE due to extensive bimolecular recombination losses. Thermal annealing does not improve hole transport in PBDTTPD BHJs but instead drastically decreases solar cell PCE. Using X-ray diffraction, we determine that the morphology of these BHJs consists of three phases: aggregated PBDTTPD, clustered PCBM, and mixed regions, which consist of PCBM dispersed in the amorphous portions of PBDTTPD. Similar three phase morphologies have been verified in several polymer-fullerene BHJ blends,[22–25] but the effect of the composition of the mixed regions on solar cell performance has not yet been investigated. With X-ray absorption techniques, we find that thermal annealing reduces the concentration of PCBM in the mixed regions of PBDTTPD BHJs. Decreasing the concentration of PCBM may reduce the number of percolating electron transport pathways within these mixed regions and create morphological electron traps that enhance charge-carrier recombination and limit device quantum efficiency. This result suggests that the composition of the mixed regions in polymer BHJs has profound effects on the performance of these solar cells. Several other high performing D-A polymer BHJ solar cells are optimal with polymer:fullerene blend ratios and active layer thicknesses similar to PBDTTPD devices.[6,9,10,12,14] Thus, we believe that the results of this study can be extended and are applicable to a wide variety of other polymer-fullerene BHJ blends.

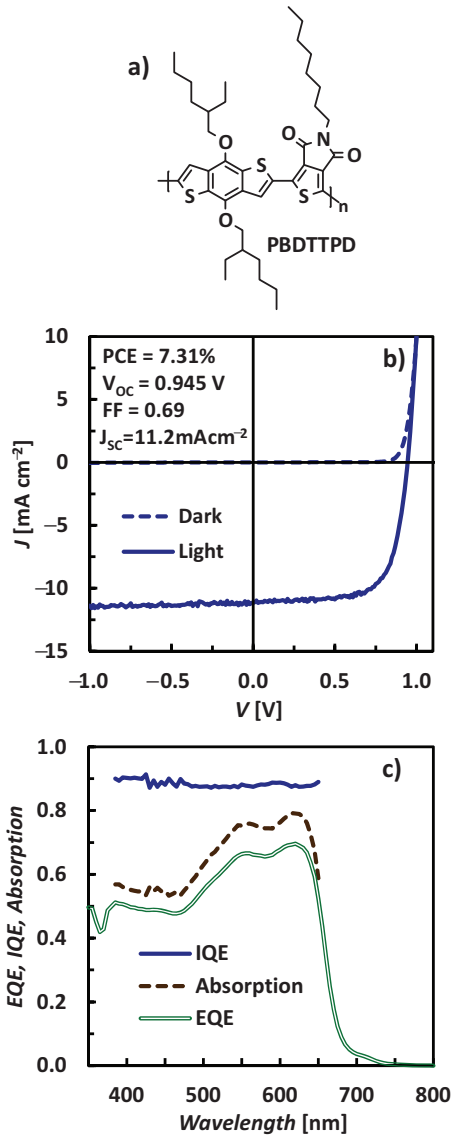

Figure 1. a) Chemical structure of PBDTTPD. b) Current density–voltage characteristics, c) quantum efficiency, and active layer absorption for optimized PBDTTPD BHJ solar cells.

2. Results and Discussion

2.1. Performance of Optimized PBDTTPD BHJ Solar Cells

Previously, 6.8%[18] and 7.1% PCE[26] were reported for PBDTTPD BHJ solar cells fabricated with a single solvent additive (1,8-diiodooctane) and co-solvent additives (1,8-diiodooctane and 1-chloronaphthalene), respectively. We recently improved upon these results and reported[21] 7.3% PCE for PBDTTPD BHJ devices (average PCE of 7.1%) placing PBDTTPD among the top performing polymers for BHJ solar cells (Figure 1b). Our optimized devices have ~100-nm-thick active layers of PBDTTPD and PCBM in a 1:1.5 weight ratio and are fabricated without the use of solvent additives, thermal annealing, or solvent annealing. The V_{OC} of these devices is ~0.95 V and is the highest reported V_{OC} for a polymer BHJ solar cell with PCE over 7%. The devices also achieve FFs near 0.70 and short-circuit currents (J_{SC}) above 11 mA cm^{-2}, which is notable because many polymer BHJ solar cells with V_{OC} near 1 V suffer from poor J_{SC} and FF.[27,28]

While optimized PBDTTPD BHJ solar cells perform exceptionally well, PBDTTPD's band gap (~1.8 eV) is higher than the optimal band gap for a single junction polymer BHJ solar

cell.[29,30] The relatively high band gap and exceptional V_{OC} and FF, however, make PBDTTPD BHJ solar cells an ideal candidate for the high band gap cell in a tandem solar cell.[31] For example, a PBDTTPD BHJ solar cell would provide a ~0.1 V improvement in voltage compared to the P3HT BHJ solar cell used as the high band gap solar cell in the current record 10.6% PCE tandem polymer solar cell.[3,32]

The quantum efficiency and active layer absorption of optimized PBDTTPD BHJ solar cells are plotted in Figure 1c. The IQE is essentially wavelength independent and is ~90%, which is similar to that of several of the highest-efficiency polymer BHJ solar cells;[6,9,33] this high IQE shows that these devices generate and collect charge-carriers from photons absorbed by both PBDTTPD and PCBM with high efficiency. Using steady-state photoluminescence (PL) measurements, we determined that 99.7% of PBDTTPD PL is quenched in as-cast PBDTTPD BHJs (Figure S1). The highly efficient PL quenching suggests that the morphology of these BHJs is finely intermixed and essentially all excitons generated in the polymer are able to reach PBDTTPD-PCBM heterojunction interfaces. We note, however, that steady-state PL quenching experiments only probe the fraction of excitons that decay radiatively and that the PL quantum efficiency of conjugated polymers can be quite low (~2% for P3HT).[34] But, the IQE of optimized PBDTTPD BHJ devices approaches ~98% when strong negative biases are applied on the devices, which verifies that nearly all excitons are in fact quenched in these devices (Figure S2). Thus, the 10% IQE loss at short-circuit in optimized devices is due to inefficiencies in charge-carrier separation and/or transport processes. The external quantum efficiency (EQE) of optimized devices peaks at ~70%, where PBDTTPD is the primary absorber. At shorter wavelengths where PCBM is the primary absorber, the EQE decreases to ~50% because the extinction coefficient of PCBM is low. Incomplete light absorption by the active layer plays a large role in limiting the EQE of these devices. Figure 1c shows that the active layer absorbs only ~80% of incident photons with wavelengths in the range of 550–650 nm and ~60% of incident photons with wavelengths in the range of 350–500 nm. This result highlights that there is room for significant PCE enhancement if light absorption in PBDTTPD BHJ solar cells can be improved without sacrificing IQE.

2.2. Bimolecular Recombination in Optically Thick Devices

Transfer matrix modeling[35] predicts that increasing the active layer thickness of PBDTTPD BHJ solar cells from 100 to 260 nm will improve the device J_{SC} by 23% and push the PCE above 8.5% (**Figure 2**a). We fabricated devices with different active layer thickness and found that 260-nm-thick devices produced 12% more current than 100-nm-thick devices at short-circuit and 18% more current at –1 V bias. While this current enhancement demonstrates that augmenting the active layer thickness does improve light absorption, the FF of the devices decreases substantially as the active layer thickness increases above 100 nm, resulting in a lower device PCE (Figure 2b, J–V curves shown in Figure S3). The strong dependence of FF on active layer thickness indicates that the built-in electric field in

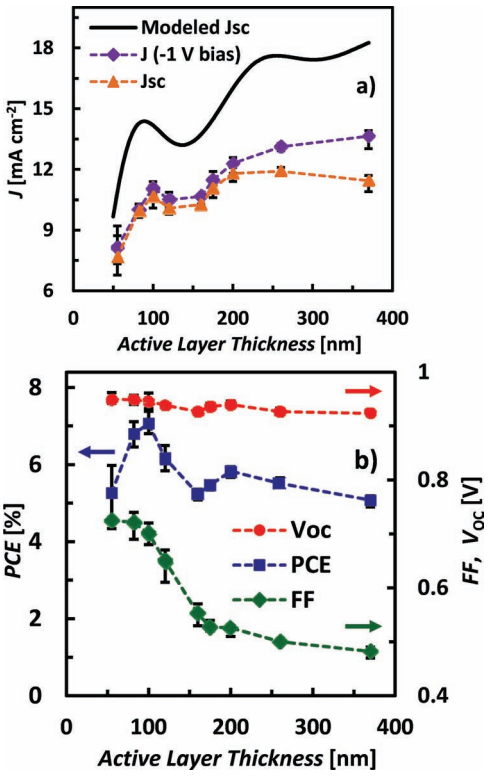

Figure 2. a) Current density vs. active layer thickness for PBDTTPD BHJ solar cells at short-circuit and with –1 V applied bias. The current density at short-circuit was also calculated from transfer matrix modeling assuming 100% IQE. b) Open-circuit voltage, power conversion efficiency, and fill factor as a function of active layer thickness for PBDTTPD BHJ solar cells. The markers denote the average values and error bars show the high and low values across several devices.

thicker-than-optimal devices is not strong enough to efficiently sweep charge-carriers out of the devices before they recombine.

To determine if recombination in optically thick devices is bimolecular in nature, we performed light intensity dependent EQE measurements (**Figure 3**). The rate of bimolecular recombination in solar cells is proportional to the product of the hole and electron concentrations in the device and consequently becomes more significant at higher light intensities. Using a low intensity monochromatic light chopped at 100 Hz and superimposed over a white light bias of varying intensity, the differential EQE, ΔEQE, was measured with a lock-in amplifier. ΔEQE represents the EQE of the additional photons supplied by the low intensity chopped light as a function of the total light intensity incident on the device. Using Equation (1), the EQE of a device at a given light intensity, I, can be determined by calculating the average ΔEQE for all photons absorbed by the device at that light intensity.

$$EQE(I) = \frac{1}{I}\int_0^I \Delta EQE(I')\, dI' \quad (1)$$

The percentage of EQE loss in the device due to bimolecular recombination at light intensity $I = I'$ can be estimated by the

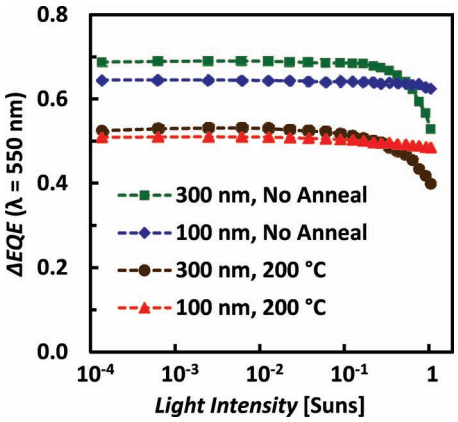

Figure 3. Differential external quantum efficiency ($\lambda = 550$ nm, at short-circuit) vs. light intensity for PBDTTPD BHJ solar cells. The data is shown for as-cast and thermally annealed (10 minutes) 100 and 300-nm-thick devices.

ratio of $EQE(I = I')$ to $EQE(I \approx 0)$. We find that at one sun light intensity (at 550 nm and short-circuit conditions) bimolecular recombination accounts for 7.8% EQE loss in 300-nm-thick devices and only 1.3% EQE loss in optimal, 100-nm-thick devices. Bimolecular recombination losses are quite small at short-circuit in optimized devices, which is expected considering these devices have ~90% IQE and ~0.70 FF. The 300-nm-thick devices, however, have substantial 7.8% EQE loss, indicating that a significant fraction of charge-carriers recombine before they are extracted from these devices, even at short-circuit when the built-in electric field in the device is much stronger than it is at the maximum power point. This bimolecular recombination problem is likely the cause of the poor FFs in optically thick PBDTTPD BHJ solar cells and may be a result of space-charge build-up due to the slow extraction of photogenerated charge-carriers.

2.3. Reduced PBDTTPD Hole Mobility in BHJs

PCBM has been shown to drastically affect hole transport in polymer BHJs, either increasing or decreasing polymer hole mobility by several orders of magnitude.[17,36] To elucidate if PCBM reduces the hole mobility in PBDTTPD BHJs, we used space-charge limited current (SCLC) measurements to determine the hole mobility in both neat PBDTTPD and PBDTTPD BHJ hole-only diodes. In our hole-only diodes we used a proprietary conducting polymer from Plextronics, CA-1914 (~5.5 eV), as the electron blocking contact to avoid evaporating a high work function metal on the active layer and used PEDOT:PSS (~5.0 eV) as the hole-injecting contact. These contacts ensured that electrons were not injected into PCBM's lowest unoccupied molecular orbital (LUMO) and that holes were efficiently injected into and extracted from PBDTTPD's highest occupied molecular orbital (HOMO, ~5.4 eV).[18] **Figure 4** shows the current density–voltage characteristics for both neat PBDTTPD and PBDTTPD BHJ hole-only diodes. Hole mobilities were determined by fitting the data to Child's Law using Equation (2), where J is the current density, V is the voltage, V_{bi} is the difference in work functions between the two contacts, L is the film thickness, and ε and μ_h are the material's dielectric constant and hole mobility, respectively.

$$J = \frac{9}{8}\varepsilon\mu_h\frac{(V - V_{bi})^2}{L^3} \quad (2)$$

Devices of a range of thickness (150–450 nm) were tested over a wide voltage range (3–15 V) to ensure that the current density was indeed space-charge limited and was properly described by Equation (2). Over ten devices were measured for each and we determined that $\mu_h = 2.0 \pm 0.7 \times 10^{-4}$ cm^2 Vs^{-1} in neat PBDTTPD and $\mu_h = 2.9 \pm 0.9 \times 10^{-5}$ cm^2 Vs^{-1} in PBDTTPD BHJs. Thus, the hole mobility in PBDTTPD decreases by a factor of seven when it is blended with PCBM in the optimal 1:1.5 weight ratio. We believe that this low hole mobility causes the extensive bimolecular recombination in optically thick PBDTTPD BHJ solar cells. The hole mobility in neat PBDTTPD is similar to the hole mobility in optimized P3HT BHJ solar cells,[17] which have minimal bimolecular recombination in devices with 220-nm-thick active layers. This comparison shows that measuring the hole mobility in a pure polymer is not sufficient to determine whether or not hole transport in a polymer-fullerene BHJ will be adequate to avoid bimolecular recombination since PCBM can hinder the polymer's hole mobility.

2.4. Three Phase Morphology of As-Cast PBDTTPD BHJs

Ideal BHJ morphologies provide complete exciton quenching, allow for highly efficient charge-carrier separation, and facilitate efficient charge-carrier transport so that electrons and holes can be quickly swept out of devices before recombining. Optimized PBDTTPD BHJ solar cells have ~90% IQE, but optically

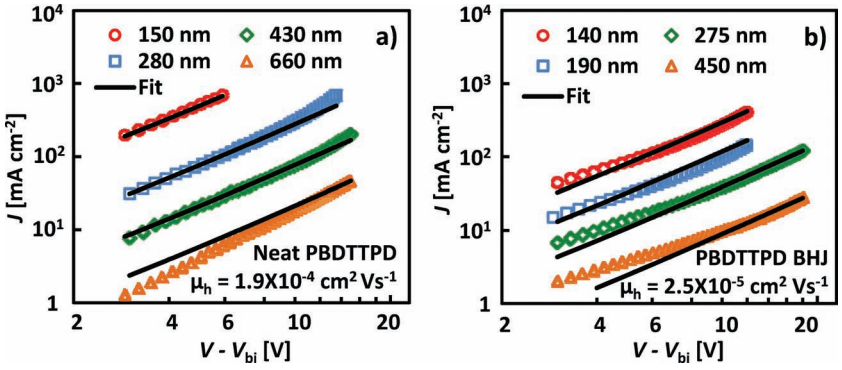

Figure 4. Current density-voltage characteristics (room temperature, in the dark) of a) neat PBDTTPD and b) PBDTTPD BHJ hole-only diodes of differing thickness. The data for all devices is simultaneously fit to Equation (2) using $V_{bi} = -0.5$ V, $\varepsilon = 3 \times 8.85 \times 10^{-14}$ F cm^{-1}, and a single fitting parameter, μ_h.

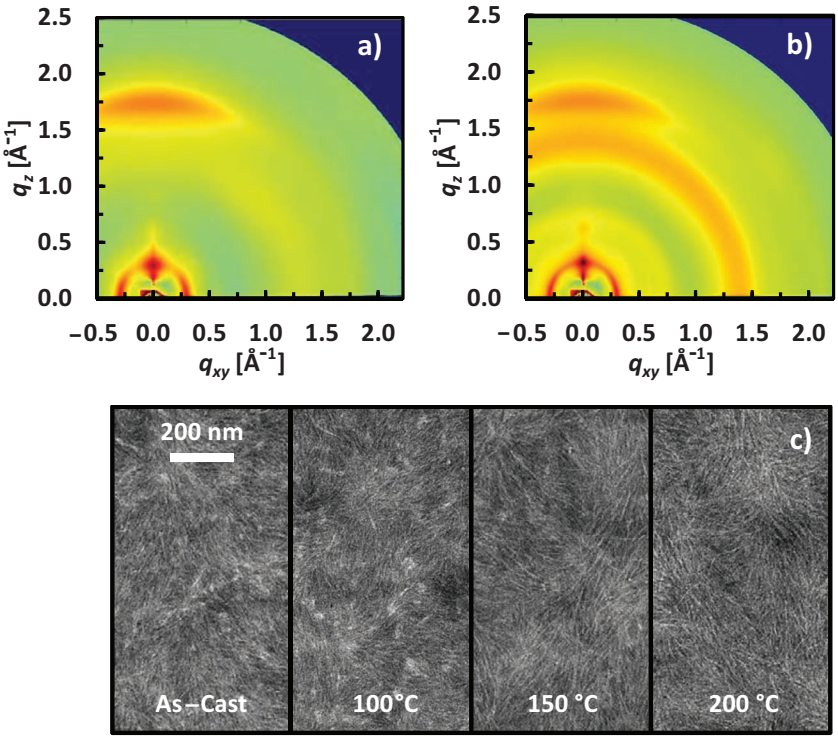

Figure 5. Two dimensional grazing incidence X-ray diffraction images of as-cast a) neat PBDTTPD and b) PBDTTPD BHJ films. Diffraction intensity is plotted on a log scale. c) Top-down bright-field transmission electron microscope images of PBDTTPD BHJs (~5 µm defocus) as-cast and thermally annealed for 10 minutes at various temperatures.

thick devices suffer from significant bimolecular recombination losses due to the low hole mobility in these BHJs. We characterized the morphology of as-cast PBDTTPD BHJs to determine both why optimized devices can attain exceptional IQE and why PCBM reduces the hole mobility in these BHJs.

To examine the molecular ordering in as-cast PBDTTPD BHJs, we performed grazing incidence X-ray diffraction (GIXD) measurements[37] on neat PBDTTPD and PBDTTPD BHJ films. Our measurements agree with those reported previously[18] with the PBDTTPD π–π stacking (q ≈ 1.7 Å^{-1}) and lamellar stacking (q ≈ 0.3 Å^{-1}) peaks in the out-of-plane and in-plane orientations, respectively (**Figure 5**). The orientation of these diffraction peaks suggests that the PBDTTPD polymer chains preferentially pack in a "face-on" orientation, but both of these peaks are smeared into partial arc shapes indicating there is a distribution of molecular orientations. Other high-efficiency D-A polymers also pack in a face-on orientation[9,15] and this orientation is thought to be advantageous for hole transport in the diode configuration.[38] The locations of the PBDTTPD diffraction peaks are not altered after blending PBDTTPD with PCBM, which indicates that PCBM does not intercalate into the diffracting, PBDTTPD domains[39] and suggests the presence of a pure PBDTTPD phase in as-cast PBDTTPD BHJs. The diffuse halos at q ≈ 0.7 Å^{-1} and q ≈ 1.4 Å^{-1} in Figure 5b are diffraction from small, amorphous PCBM clusters[40] and verify the presence of a pure PCBM phase in these BHJs. Transmission electron microscope (TEM) images show small fibrillar domains in as-cast PBDTTPD BHJs (Figure 5c). Similar morphologies have been observed in other non-intercalating polymer BHJ systems,[41,42] and we infer that these fibrils are composed of PBDTTPD because pure PBDTTPD domains should appear brightest in bright-field TEM images (PBDTTPD has a lower electron density than PCBM), and fibrillar features are present in pure PBDTTPD films but not in pure PCBM films (Figure S4). While this result further supports the presence of small, pure PBDTTPD domains in these BHJs, additional experiments would be needed to determine the composition of these domains and verify that they do not contain any PCBM.[42]

The large radial breadth of the PBDTTPD diffraction peaks and absence of higher-order and mixed-index diffraction peaks indicate that the diffraction from PBDTTPD is due to relatively short-range molecular order and not long-range order. This observation suggests that the overall degree of order in PBDTTPD BHJs is low compared to BHJs made with more crystalline polymers like P3HT or poly(2,5-bis(3-alkylthiophen-2-yl) thieno[3,2-*b*]thiophene) (PBTTT).[39,40] Furthermore, the degree of molecular order within the pure PBDTTPD domains can be probed by calculating the paracrystallinity parameter, *g*, which is a measure of the statistical deviation from the mean lattice spacing in a crystal. For reference, $g = 0\%$ for a perfect crystal, $g \approx 1\%$ for specular diffraction in highly textured 6,13-bis(triisopropylsilylethynyl) pentacene (TIPS-pentacene), $g \approx 7\%$ for the π–π stacking in aligned PBTTT, and $g \approx 12\%$ for amorphous silicon dioxide (SiO_2) glass.[43,44] Rivnay et al.[43] showed that *g* can be estimated in systems where disorder dominates peak broadening effects using Equation (3), where Δ_q and d_{hkl} are the full width at half maximum (FWHM) and interplanar spacing for the diffraction peak of interest, respectively.

$$g \approx \frac{1}{2\pi}\sqrt{\Delta_q d_{hkl}} \tag{3}$$

With Equation (3) we estimate that $g \approx 14\%$ for the π–π stacking and $g \approx 11\%$ for the lamellar stacking in the pure polymer domains in as-cast PBDTTPD BHJs. This analysis shows that the PBDTTPD domains in these BHJs are largely disordered since their paracrystallinity parameter is more comparable to SiO_2 glass than to crystals of ordered molecules like TIPS-pentacene or PBTTT. Thus, we find that the pure PBDTTPD domains are more accurately described as "disordered polymer aggregates" rather than as "polymer crystals" with finite grain sizes.

The hole mobility in semiconducting polymers has been correlated with the orientation of the polymer π–π stacking,[45] the π–π stacking paracrystallinity (or coherence length),[15] the polymer degree of aggregation (or crystallinity),[46] and the degree of polymer backbone alignment.[47] In the GIXD images in Figure 5, we see that the PBDTTPD π–π stacking diffraction

peak at q ≈ 1.7 Å^{-1} is preferentially oriented out of plane in both the neat PBDTTPD and PBDTTPD BHJ samples, and the angular dependence of the peak intensity for each sample is similar. This result indicates that PCBM does not significantly alter the orientation of the PBDTTPD π–π stacking. Using Equation (3), we also estimate that the π–π stacking paracrystallinity is ~14% in both neat PBDTTPD and PBDTTPD BHJs, which indicates that PCBM does not significantly affect the π–π stacking order within the pure PBDTTPD aggregates. The degree of aggregation of a polymer film affects the hole mobility because hole transport in semiconducting polymer films can be aided by the presence of percolating pathways of crystalline or aggregated polymer domains.[46] We hypothesize that the hole mobility in PBDTTPD BHJs is lower than the hole mobility in neat PBDTTPD because there are fewer percolating aggregated PBDTTPD pathways in the BHJs compared to the neat PBDTTPD films. Hammond et al.[48] and Turner et al.[49] recently determined that fullerenes significantly decrease the degree of polymer aggregation in as-cast BHJs based on PTB7[9] (a high performing D-A polymer) and P3HT, respectively. A quantitative assessment of the degree of aggregation in PBDTTPD films is beyond the scope of this work, but we suggest that PCBM inhibits PBDTTPD aggregation in as-cast BHJs. Thus, PCBM reduces the hole mobility in PBDTTPD, and bimolecular recombination limits the active layer thickness of PBDTTPD BHJ solar cells.

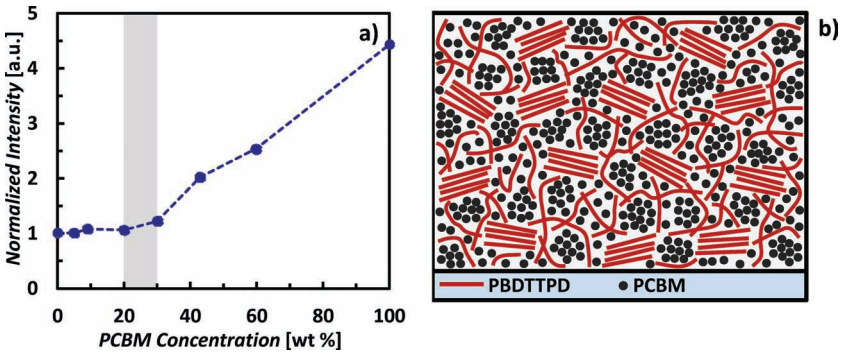

Figure 6. a) Normalized grazing incidence X-ray diffraction intensity (q ≈ 0.7 Å^{-1}) as a function of the PCBM concentration in PBDTTPD BHJs. The data is normalized by the background diffraction intensity for each sample, and the gray rectangle marks the estimated as-cast concentration of PCBM mixed in PBDTTPD. b) Morphology schematic of an as-cast PBDTTPD BHJ (the volume fraction of each phase is estimated).

Fullerenes are known to mix in the amorphous portions of semicrystalline polymers in several polymer-fullerene BHJ systems.[25,50–53] Since we believe the degree of aggregation in as-cast PBDTTPD BHJs is relatively low, there is likely a significant fraction of amorphous PBDTTPD in these BHJs. To determine the extent of polymer-fullerene mixing, we examined the GIXD intensity as a function of PBDTTPD BHJ composition (**Figure 6**a). At q ≈ 0.7 Å^{-1} there is negligible diffraction from PBDTTPD, and any diffraction intensity above the background is solely due to diffraction from PCBM clusters (cake segments in Figure S5). The absence of PCBM diffraction intensity at q ≈ 0.7 Å^{-1} in as-cast PBDTTPD BHJs with PCBM concentrations less than 20 wt% shows that PCBM and PBDTTPD are well mixed at these compositions and form a phase consisting of PCBM dispersed in the amorphous portions of PBDTTPD. As the PCBM concentration is increased above 20 wt%, the diffraction intensity at q ≈ 0.7 Å^{-1} increases linearly indicating that pure PCBM clusters begin to form in blends with PCBM concentrations greater than 20 wt% (Figure 6a). We fit the data points from 0 to 20 wt% PCBM and 30 to 100 wt% PCBM with linear regressions and define the as-cast concentration of PCBM mixed in PBDTTPD as the intersection of these two lines of best fit. It should be noted that this method measures the concentration of PCBM mixed in the total mass of PBDTTPD, including both the aggregated and amorphous portions; the concentration of PCBM in the amorphous portions of PBDTTPD is higher than the measured value since PCBM does not intercalate into the PBDTTPD aggregates. Thus, we find that in as-cast PBDTTPD BHJs the concentration of PCBM mixed in the amorphous portions of PBDTTPD is at least 25 ± 5 wt%, where the error is due to uncertainty in the linear fits.

Using this analysis, we conclude that the as-cast morphology of PBDTTPD BHJs consists of three phases: 1) disordered PBDTTPD aggregates, 2) amorphous, clustered PCBM, and 3) molecularly-mixed amorphous PBDTTPD and PCBM. Figure 6b shows a schematic of the as-cast morphology of PBDTTPD BHJs. Three phase BHJ morphologies have been observed in other BHJ systems and may be advantageous for BHJ solar cell operation for several reasons.[22–25] First, the aggregated PBDTTPD and clustered PCBM domains may act as high mobility hole and electron transporting pathways in the BHJ, respectively.[24] It has been shown in other polymer-fullerene BHJ systems that pure fullerene domains are necessary for efficient electron transport,[39] and, as noted previously, hole transport in semiconducting polymers is aided by percolating aggregated or crystalline polymer domains.[46] Furthermore, it is advantageous to have relatively small PBDTTPD and PCBM domains because large domains can reduce exciton quenching efficiency.[54,55] Secondly, intimately molecularly-mixed regions with adequate carrier mobility allow for both highly efficient exciton quenching and charge-carrier extraction. Given that optimized PBDTTPD BHJ solar cells have ~90% IQE, charge-carriers generated in the mixed regions are efficiently separated and extracted from these devices. We propose that this extraction process is efficient because there is an energetic driving force for electrons and holes to leave the mixed regions and travel into and through the clustered PCBM and aggregated PBDTTPD domains, respectively. More specifically, electrons lower their energy by travelling from the mixed regions to the clustered PCBM domains because the electron affinity of the clustered PCBM domains may be higher than that of the PCBM in the mixed regions, as was determined by Jamieson et al.[25] Conversely, holes lower their energy by travelling from the mixed regions into the aggregated PBDTTPD domains, which likely have longer conjugation lengths and lower ionization potentials than the amorphous PBDTTPD in the mixed regions.[56] This mechanism of hole transfer from amorphous to aggregated polymer regions was recently verified experimentally in semicrystalline P3HT films.[57]

2.5. Thermal Annealing Creates Morphological Electron Traps

Thermal and solvent annealing improve the PCE of P3HT BHJ solar cells from less than 2% to greater than 4% by drastically improving the FF and J_{SC}; these effects are attributed primarily to improvements in polymer ordering and hole mobility.[16,17] In an attempt to improve hole transport and enhance the PCE of optically thick PBDTTPD BHJ solar cells, we thermally annealed devices for 10 minutes at temperatures above and below the glass transition temperature ($T_g \approx 138$ °C)[19] of PBDTTPD. Thermal annealing at all temperatures decreased the PCE in both 100-nm-thick and optically thick devices primarily due to decreases in J_{SC} and to a lesser extent in FF (**Figure 7**a). The PCE degradation became progressively more pronounced as the thermal annealing temperature was increased with the 200 °C anneal decreasing the J_{SC} and PCE by 20% and 30%, respectively. Previous studies on other polymer-fullerene BHJ systems have demonstrated that thermal annealing can decrease solar cell PCE; most often it is concluded that thermal annealing decreases device photocurrent because it drives phase separation and reduces the amount of interfacial area between the donor and acceptor materials, which inhibits exciton quenching.[58,59] We performed steady-state PL quenching experiments and verified that the PBDTTPD PL is still 98.7% quenched after thermal annealing PBDTTPD BHJs with both 60 wt% and 43 wt% PCBM at 200 °C for up to 60 minutes (Figure S1). Thus, the 20% decrease in J_{SC} after thermal annealing PBDTTPD BHJ solar cells is not caused by decreases in exciton dissociation efficiency, although this result may not be the case for other BHJ blends.

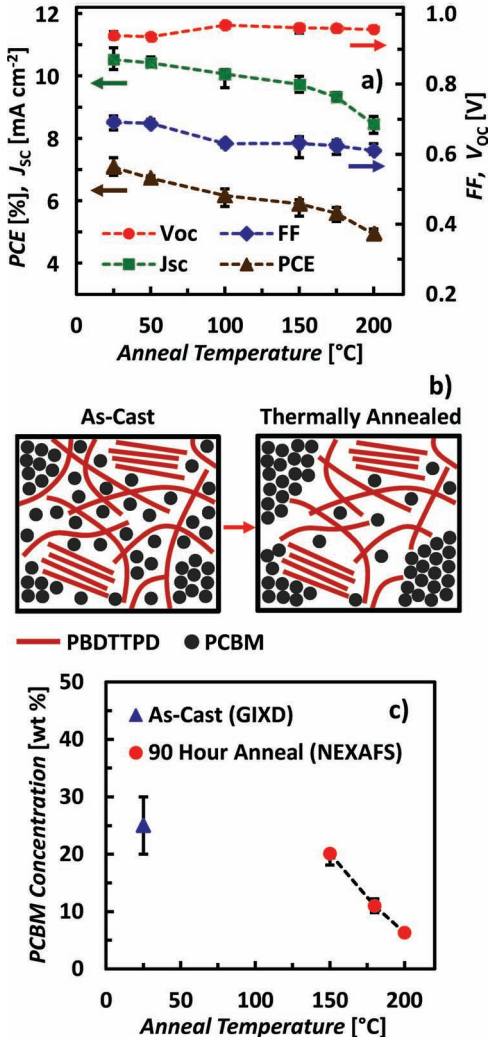

Figure 7. a) PBDTTPD BHJ solar cell performance vs. thermal anneal temperature (10 minutes anneals, ~100-nm-thick devices). Similar trends were observed in optically thick devices. The markers denote the average value and error bars denote the high and low values across several devices. b) Schematic of the PBDTTPD BHJ morphology before and after thermal annealing. c) Concentration of PCBM mixed in PBDTTPD as a function of temperature.

We propose that thermal annealing decreases the J_{SC} and PCE of PBDTTPD BHJ solar cells because it drives PCBM to diffuse out of the mixed regions in these BHJs and into pure PCBM domains (Figure 7b). As a result, the number of PCBM pathways that percolate throughout the amorphous PBDTTPD matrix may be reduced. Without these percolating PCBM pathways, electrons in the mixed regions would have to hop large distances across polymer molecules from one isolated PCBM molecule (or small cluster) to another in order to drift under an applied electric field. This hopping process would be exceedingly slow, and the electrons would likely quickly recombine with nearby holes. Thus, the isolated PCBM molecules in the non-percolated mixed regions would act as "morphological electron traps," because any electrons transferred to these isolated molecules would be effectively trapped and would have a negligible drift velocity. The hypothesis that isolated PCBM molecules in polymer BHJs act as charge-carrier traps has been proposed previously,[24,50,60] but the effects of these traps on solar cell performance have not yet been investigated. In our morphological electron trap model, thermal annealing and trap formation does not significantly affect the number of photons absorbed or the number of excitons dissociated in the solar cells. Thermal annealing instead affects the ability to extract charge-carriers from the mixed regions in these devices.

To verify our hypothesis, we examined the miscibility of PCBM in PBDTTPD as a function of temperature. The as-cast concentration of PCBM mixed in PBDTTPD was measured from GIXD as described previously. The PCBM concentration at elevated temperatures, however, was measured using a method[61] in which the near-edge X-ray absorption fine structure (NEXAFS) spectrum of the mixed regions was quantitatively fit using a combination of the NEXAFS spectra of pure PBDTTPD and PCBM. For this measurement, the PBDTTPD BHJ samples were thermally annealed at their respective temperatures for 90 hours to ensure the mixed regions in each sample had adequate time to approach their equilibrium composition and to ensure that the PCBM-depleted regions were sufficiently large enough (>100 nm laterally) to accurately measure the composition of the mixed regions with NEXAFS due to the limited lateral resolution of the focused X-ray beam.[61] The PCBM concentration was then determined by measuring the composition of the PCBM-depleted mixed regions surrounding the large PCBM clusters that were formed in the thermally annealed

samples (Figure S6). As with the GIXD PCBM concentration measurement, this technique measures the concentration of PCBM mixed in the total mass of PBDTTPD, including both the amorphous and aggregated portions. While the morphology obtained after spin-casting may be metastable, it is still instructive to compare the as-cast PCBM concentration measured by GIXD to that measured by NEXAFS at elevated temperature because it provides an idea of how the BHJ morphology will tend to evolve during thermal annealing.

We find that the concentration of PCBM mixed in PBDTTPD is reduced significantly as the temperature is increased, decreasing from ~25 wt% as-cast to ~6 wt% at 200 °C (Figure 7c). The trend of decreasing PCBM and polymer miscibility with increasing temperature has not yet been observed in other BHJ systems,[50] and two component mixtures often become more miscible as temperature is increased because the entropic gains associated with mixing begin to overcome the enthalpic penalties of mixing at higher temperatures. While a comprehensive examination of the thermodynamics of mixing in this system is beyond the scope of this work, the most important finding is that the miscibility of PCBM in PBDTTPD clearly decreases as the temperature is increased. This behavior implies there is a driving force at elevated temperatures for PCBM to diffuse out of the mixed regions of as-cast PBDTTPD BHJs and either contribute to the growth of the PCBM clusters present in as-cast films or nucleate small PCBM clusters within the mixed regions. Although the 90 hour thermal anneals used for the NEXAFS composition measurements are much longer than the 10 minute thermal anneals used for solar cell fabrication, significant fullerene diffusion has been observed on times scales as short as 10 seconds in P3HT and PCBM bilayers[62] and P3HT BHJs[63] at similar thermal anneal temperatures. Thus, we believe it is reasonable to assume that PCBM will diffuse out of the mixed regions adjacent to the PCBM clusters in PBDTTPD BHJ solar cells after 10 minutes of thermal annealing. The size of the PCBM-depleted mixed regions formed after only 10 minutes of thermal annealing, however, is much smaller than that obtained after 90 hours of annealing (>1 μm wide, Figure S6) since the PCBM diffusion length is proportional to the square root of the thermal anneal time.

Vakhshouri et al.[64] recently showed that the transistor electron mobility in BHJs of regiorandom P3HT (RRa-P3HT) and PCBM is described by percolation theory and is highly sensitive to the PCBM concentration. In this study, they estimated the percolation threshold for electron transport in RRa-P3HT as ~20 wt% PCBM and showed that the electron mobility in RRa-P3HT BHJs with <20 wt% PCBM is negligible (μ_e < 10^{-10} cm^2 Vs^{-1}). We speculate that the electron mobility in the mixed regions of PBDTTPD BHJs likely behaves similarly to that of RRa-P3HT BHJs because both systems consist of the same electron transporting material, PCBM, mixed in an amorphous polymer matrix. The 25 ± 5 wt% concentration of PCBM mixed in PBDTTPD in as-cast BHJs (as determined by GIXD) is above the ~20 wt% PCBM percolation threshold for electron transport determined by Vakhshouri et al. The measured PCBM concentrations for the 150 °C (20 wt%), 180 °C (11 wt%), and 200 °C (6 wt%) thermally annealed PBDTTPD BHJs, however, either just meet or are below this percolation threshold. We note again that the concentration of PCBM mixed in the amorphous portions of the PBDTTPD is actually higher than these measured concentrations because the aggregated PBDTTPD domains exclude PCBM. But, unrealistically high degrees of PBDTTPD aggregation (45% and 70%) would be needed for the concentration of PCBM in the amorphous portions of PBDTTPD to just reach the 20 wt% percolation threshold in the 180 and 200 °C samples, respectively. Thus, we infer that the mixed regions surrounding the PCBM clusters in thermally annealed PBDTTPD BHJs are depleted of PCBM and have poorly connected PCBM networks. These PCBM-depleted mixed regions likely have isolated PCBM molecules surrounded by PBDTTPD and dead ends in the PCBM network, which act as morphological electron traps and make electron transport inefficient. On the other hand, the more fullerene-rich mixed regions in the as-cast BHJs likely have well-connected PCBM networks, which can efficiently transport electrons from the mixed regions to the pure PCBM phase and the device contacts.

The EQE spectra of thermally annealed PBDTTPD solar cells show losses that are consistent with our morphological electron trapping model (**Figure 8**). For this analysis, we examined ~260-nm-thick devices to amplify all recombination losses, but similar trends were also observed in 100-nm-thick devices. As shown in Figure 8a, thermal annealing decreases the EQE across all wavelengths, indicating that charge-carriers are lost from photons generated by both PBDTTPD and PCBM absorption. This broadband decrease in EQE supports the morphological electron trap model because any electron generated from an exciton dissociated at the interface of a morphological electron trap is trapped whether that exciton was generated in PCBM or PBDTTPD. Additionally, the magnitude of the EQE loss increases with increasing thermal annealing temperature, which matches the trend in J_{SC} loss observed in Figure 7a. This trend indicates that the number of morphological traps in thermally annealed devices increases as the annealing temperature increases and the concentration of PCBM in the mixed regions is decreased (Figure 7c). We expect the number of morphological

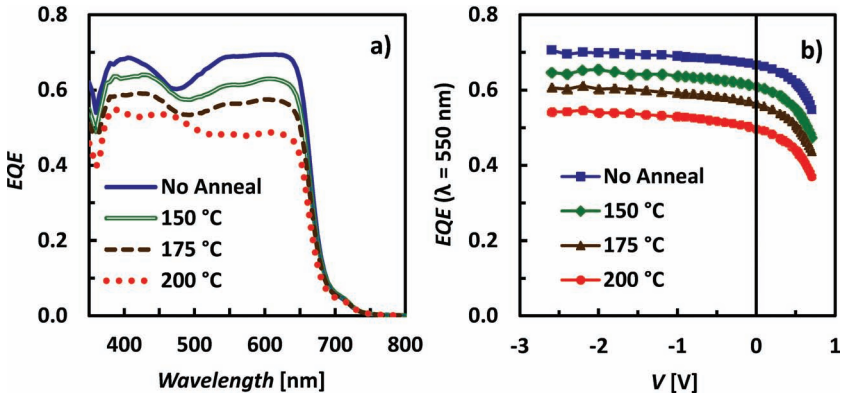

Figure 8. a) External quantum efficiency vs. wavelength and b) external quantum efficiency (λ = 550 nm) vs. applied bias for thermally annealed PBDTTPD BHJ solar cells (10 minutes anneals, ~260-nm-thick devices).

electron traps to increase as the concentration of PCBM decreases because the number of percolating PCBM pathways throughout the mixed regions would likely be further reduced, leaving more isolated PCBM molecules in these regions. Additionally, because diffusion coefficients increase exponentially with temperature, PCBM likely diffuses most quickly in the PBDTTPD BHJs thermally annealed at the highest temperatures; thus, the volume of the PCBM-depleted mixed regions (and number of morphological traps) in the thermally annealed devices should increase with increasing annealing temperature. Figure 8b shows the EQE as a function of bias applied on the same thermally annealed PBDTTPD solar cells. We find that the EQE lost after thermal annealing cannot be fully recovered, even when a negative bias is applied on the devices. This result suggests that there are trapped charge-carriers in the thermally annealed devices, which cannot be extracted and collected from the devices. Our morphological trap model is consistent with this result because electrons trapped on isolated PCBM molecules in the mixed regions of thermally annealed devices likely have negligible mobility ($\mu_e < 10^{-10}$ cm^2 Vs^{-1}). Thus, these trapped electrons cannot be swept out of the mixed regions in these devices by an electric field and recombine with holes regardless of the applied bias. The J-V curves of both 100-nm-thick and 260-nm-thick thermally annealed devices (Figure S7) have relatively bias-independent currents in reverse bias, which further verifies this finding.

The primary effects of thermal annealing on PBDTTPD BHJ solar cell performance are fundamentally different from those observed in some other polymer BHJ systems. In PCDTBT BHJ solar cells, thermal annealing decreases device PCE because it significantly decreases the PCDTBT π–π stacking coherence and hole mobility.[15] The reduction in PCDTBT structural order predominantly leads to large decreases in device FF and PCE, but all trapped charge-carriers in the annealed devices can be recovered with sufficient reverse bias. We examined the PBDTTPD BHJ morphology and hole mobility after thermal annealing and verified that a similar mechanism was not significant in PBDTTPD BHJ devices. We found that thermal annealing only decreased the PBDTTPD π–π stacking coherence in PBDTTPD BHJs moderately (Figure S8) and did not significantly affect the SCLC hole mobility in PBDTTPD BHJ hole-only diodes (data not shown). Additionally, GIXD (Figure S9 and S10) confirmed that the orientation of the PBDTTPD domains was only changed slightly by thermal annealing (population of face-on oriented domains increased) and TEM (Figure 2c) confirmed that the size and shape of the PBDTTPD domains were not significantly altered by thermal annealing. These results confirm that only small-scale PBDTTPD morphology changes occur in PBDTTPD BHJs after 10 minutes of thermal annealing. We also performed light intensity dependent EQE measurements to examine bimolecular recombination losses in thermally annealed PBDTTPD BHJ solar cells (Figure 5). Thermal annealing at 200 °C for 10 minutes only increased the amount of EQE lost to bimolecular recombination from 1.3% to 3.1% in 100-nm-thick devices and 7.8% to 11.6% in 300-nm-thick devices. The relatively small increase in bimolecular recombination after thermal annealing shows that the overall bulk charge-carrier mobilities are not significantly affected by thermal annealing and illustrates that the non-trapped charge-carriers in these devices are extracted with efficiency similar to as-cast devices. Lastly, we verified that the absorption of PBDTTPD BHJ solar cells was not affected by thermal annealing, and thus conclude that PCBM diffusion and morphological trap formation are likely the primary cause of the PCE decrease in thermally annealed PBDTTPD BHJ devices.

3. Conclusions

Making thicker PBDTTPD BHJ solar cells to increase light absorption could potentially increase device PCE from 7.3% to over 8.5%, but the active layer thickness of these devices is limited by bimolecular recombination. Thermal annealing does not improve charge transport in PBDTTPD BHJs and reduces solar cell PCE because it significantly decreases the concentration of PCBM mixed in the amorphous portions of PBDTTPD. The concentration of PCBM in these mixed regions must be well above the percolation threshold for efficient electron transport, or else isolated PCBM molecules surrounded by PBDTTPD can act as morphological electron traps and enhance charge-carrier recombination. Thus, the development of novel processing techniques, which improve PBDTTPD hole mobility while maintaining PCBM percolation in the mixed regions, is necessary to minimize bimolecular recombination losses in optically thick devices and maximize the PCE of PBDTTPD BHJ solar cells. Given that many high-efficiency D–A polymers are largely disordered[8,15,48] and polymer-fullerene mixing is commonplace,[25,50–53,65] these findings likely apply to a variety of BHJ systems. This work highlights that even if a polymer BHJ solar cell has complete exciton quenching, highly efficient charge-carrier separation, and high bulk charge-carrier mobility, near unity IQE can only be attained if there is a well-connected PCBM network in the mixed regions of the device.

These findings also have implications for polymer BHJ solar cell reliability. PBDTTPD BHJ solar cells lose PCE when thermally annealed at temperatures as low as 50 °C. This result illustrates that PCBM diffusion can occur in BHJs made with high T_g polymers at temperatures reached during outdoor solar cell operation. Thus, the PCE of polymer BHJ solar cells may be adversely affected by morphological electron trap formation after outdoor use if the equilibrium polymer-fullerene miscibility is below that needed for fullerene percolation. This finding suggests that BHJ systems with high equilibrium polymer-fullerene miscibility[22,39,51] should be used or novel methods like polymer cross-linking[66,67] should be employed to limit fullerene diffusion and improve the morphological thermal stability of polymer BHJ solar cells.

4. Experimental Section

Device Preparation: Glass substrates patterned with ITO (15 Ω/square, Xinyan Technologies LTD) were scrubbed with a dilute Extran 300 detergent, ultrasonicated in dilute Extran 300 detergent for 15 min, rinsed in de-ionized (DI) water for 5 min, sequentially ultrasonicated in acetone and isopropyl alcohol baths for 15 min, and exposed to a UV-ozone plasma for 15 min. An aqueous solution of PEDOT:PSS (Clevios P VP AI 4083) was spin-cast at 4,000 rpm onto the substrates and baked at 140 °C for 10 min. Substrates were next transferred into a dry nitrogen glovebox (<3 ppm O_2). PBDTTPD was synthesized as described in the Supplementary Information and PCBM was purchased

from Nano-C. Solutions (all in chlorobenzene, purchased from Sigma-Aldrich) were prepared in the glovebox and active layers were spin-cast at 115 °C after the solutions were allowed to dissolve overnight at 115 °C. Optimized solar cells used 8 mg PBDTTPD ml^{-1} - 12 mg PCBM ml^{-1} solutions and were spin-cast at 1,200-1,300 rpm for 45 seconds (500 rpm s^{-1}). All thermal annealing was done in the glovebox prior to electrode deposition. Electrodes were thermally evaporated at ~1×10^{-6} torr (7 nm of calcium and 150 nm of aluminum, metals purchased from Plasmaterials and K. J. Lesker, respectively). For hole-only diodes, a film of CA-1914 (Plextronics, diluted 50% by volume with ethanol) was spin-cast onto the active layer at 4,000 rpm (in the air, in the dark) and baked at 65 °C for 15 min before thermally evaporating ~150 nm of aluminum for the top electrode. Hole-only diodes of neat PBDTTPD were also prepared with aluminum instead of CA-1914 to ensure that exposure to air and low temperature thermal annealing did not significantly affect the PBDTTPD hole mobility. The active area of all solar cells and diodes was 0.1 cm^2.

Device Characterization: Current density–voltage measurements were performed in a dry nitrogen glovebox using a Keithley 2400 source meter and a Spectra-Physics 91160-1000 solar simulator (calibrated to 1 sun, AM1.5 G, with a NREL certified KG-5 filtered silicon photodiode). EQE was also measured in the glovebox and a halogen lamp (intensity calibrated with a KG-5 photodiode) was used for the white light bias when needed. A Stanford Research Systems model SR830 DSP lock-in amplifier was used to measure the EQE when the samples were irradiated with a chopped monochromatic light. Active layer optical constants were measured with a Woollam M2000 spectroscopic ellipsometer and film thicknesses were measured with a Veeco Dektak profilometer. To calculate the IQE, the device absorption was measured with an integrating sphere to collect scattered light, and the active layer absorption was isolated by subtracting parasitic electrode absorptions, calculated by transfer matrix modeling, from the total device absorption.[68] Current density–voltage measurements for the hole-only diodes were not corrected for potential loss due to series resistance as this correction was small for the measurement range used.

PL Quenching: Active layers were spin-cast onto cleaned glass slides using the procedures outlined previously. An Ar-ion laser (λ = 488 nm) was used to illuminate the samples in a nitrogen-filled chamber and PL was measured with a Princeton Instruments spectrophotometer with a silicon CCD detector that was corrected for the instrument response. PL data was normalized by the film optical density, which was measured in air using an Ocean Optics DT-1000-CE UV-Vis spectrometer. PL quenching efficiency was determined by dividing the spectrally integrated PL intensity of a blend film by that of a pure polymer film processed in a similar manner.

GIXD: Active layers were spin-cast onto PEDOT:PSS-coated silicon substrates using the procedures outlined previously. GIXD experiments were carried out at the Stanford Synchrotron Radiation Lightsource beamline 11-3 using photon energy of 12.7 keV, a MAR345 image plate area detector, a helium-filled sample chamber, and an incident X-ray beam angle of ~0.12°.

TEM: Active layers were spin-cast onto PEDOT:PSS-coated silicon substrates using the procedures outlined previously. The films were then floated off the substrates by dissolving the PEDOT:PSS in DI-water and were collected on lacey carbon coated TEM grids. TEM characterization was performed on a FEI Tecnai T12 transmission electron microscope in bright-field mode with an accelerating voltage of 120 keV.

NEXAFS and STXM: Active layers were spin-cast onto poly(styrene)-co-styrene sodium sulfonate (NaPSS)-coated glass substrates. A 1:1 PBDTTPD:PCBM weight ratio was used because it produced films with the easily discernible PCBM clusters. The films were thermally annealed in a nitrogen glovebox environment enclosed in a chamber over a hotplate. The temperature was monitored via a NIST-calibrated surface thermometer. The samples were quickly quenched to room temperature by placing the samples on an aluminum block. The films were floated off the substrates by dissolving the NaPSS layer in DI-water and were placed on copper TEM grids. NEXAFS and STXM experiments were carried out at the Advanced Light Source at Lawrence Berkeley National Laboratory beamline 5.3.2.2.[69] All NEXAFS measurements were taken in transmission mode to ensure that the bulk composition of the thin film samples was probed.

Supporting Information

Supporting Information is available from the Wiley Online Library or from the author.

Acknowledgements

The authors acknowledge Nichole Cates Miller, Sean Sweetnam, Kristin Schmidt, and Christopher Tassone for helpful discussions and thank Plextronics for supplying the CA-1914. This publication was based on work supported by the Center for Advanced Molecular Photovoltaics (CAMP) (Award No KUS-C1-015-21), made by King Abdullah University of Science and Technology (KAUST). J.A.B. and Z.M.B. acknowledge government support under and awarded by the DoD, Air Force Office of Scientific Research, National Defense Science and Engineering Graduate (NDSEG) Fellowship, 32 CFR 168a. E.T.H acknowledges funding from the Fannie and John Hertz Foundation. The NEXAFS miscibility study by NCSU was supported by DOE contract DE-FG02-98ER45737. Portions of this research were carried out at the Stanford Synchrotron Radiation Lightsource user facility, operated by Stanford University on behalf of the U.S. Department of Energy, Office of Basic Energy Sciences and at the Advanced Light Source, Berkeley, which is supported by the Director, Office of Science, Office of Basic Energy Sciences, of the U.S. Department of Energy under Contract DE-AC02- 05CH11231.

Received: August 14, 2012
Revised: September 3, 2012
Published online: October 26, 2012

[1] G. Yu, J. Gao, J. C. Hummelen, F. Wudl, A. J. Heeger, *Science* **1995**, *270*, 1789.
[2] M. A. Green, K. Emery, Y. Hishikawa, W. Warta, E. D. Dunlop, *Prog. Photovolt.: Res. Appl.* **2012**, *20*, 12.
[3] NREL, Best Research-Cell Efficiencies, http://www.nrel.gov/ncpv/images/efficiency_chart.jpg, (accessed September, **2012**).
[4] P.-L. T. Boudreault, A. Najari, M. Leclerc, *Chem. Mater.* **2011**, *23*, 456.
[5] D. Mühlbacher, M. Scharber, M. Morana, Z. Zhu, D. Waller, R. Gaudiana, C. J. Brabec, *Adv. Mater.* **2006**, *18*, 2884.
[6] H.-Y. Chen, J. Hou, S. Zhang, Y. Liang, G. Yang, Y. Yang, L. Yu, Y. Wu, G. Li, *Nature Photon.* **2009**, *3*, 649.
[7] M. Lenes, G.-J. A. H. Wetzelaer, F. B. Kooistra, S. C. Veenstra, J. C. Hummelen, P. W. M. Blom, *Adv. Mater.* **2008**, *20*, 2116.
[8] J. Peet, J. Y. Kim, N. E. Coates, W. L. Ma, D. Moses, A. J. Heeger, G. C. Bazan, *Nat. Mater.* **2007**, *6*, 497.
[9] Y. Liang, Z. Xu, J. Xia, S.-T. Tsai, Y. Wu, G. Li, C. Ray, L. Yu, *Adv. Mater.* **2010**, *22*, E135.
[10] C. M. Amb, S. Chen, K. R. Graham, J. Subbiah, C. E. Small, F. So, J. R. Reynolds, *J. Am. Chem. Soc.* **2011**, *133*, 10062.
[11] T.-Y. Chu, S. Alem, S.-W. Tsang, S.-C. Tse, S. Wakim, J. Lu, G. Dennler, D. Waller, R. Gaudiana, Y. Tao, *Appl. Phys. Lett.* **2011**, *98*, 253301.
[12] T.-Y. Chu, J. Lu, S. Beaupré, Y. Zhang, J.-R. Pouliot, S. Wakim, J. Zhou, M. Leclerc, Z. Li, J. Ding, Y. Tao, *J. Am. Chem. Soc.* **2011**, *133*, 4250.
[13] S. C. Price, A. C. Stuart, L. Yang, H. Zhou, W. You, *J. Am. Chem. Soc.* **2011**, *133*, 4625.
[14] L. Huo, S. Zhang, X. Guo, F. Xu, Y. Li, J. Hou, *Angew. Chem., Int. Ed.* **2011**, *50*, 9697.

[15] Z. M. Beiley, E. T. Hoke, R. Noriega, J. Dacuña, G. F. Burkhard, J. A. Bartelt, A. Salleo, M. F. Toney, M. D. McGehee, *Adv. Energy Mater.* **2011**, *1*, 954.
[16] G. Li, V. Shrotriya, J. Huang, Y. Yao, T. Moriarty, K. Emery, Y. Yang, *Nat. Mater.* **2005**, *4*, 864.
[17] V. D. Mihailetchi, H. X. Xie, B. de Boer, L. J. A. Koster, P. W. M. Blom, *Adv. Funct. Mater.* **2006**, *16*, 699.
[18] C. Piliego, T. W. Holcombe, J. D. Douglas, C. H. Woo, P. M. Beaujuge, J. M. J. Fréchet, *J. Am. Chem. Soc.* **2010**, *132*, 7595.
[19] Y. Zou, A. Najari, P. Berrouard, S. Beaupré, B. R. Aich, Y. Tao, M. Leclerc, *J. Am. Chem. Soc.* **2010**, *132*, 5330.
[20] Y. Zhang, S. K. Hau, H.-L. Yip, Y. Sun, O. Acton, A. K.-Y. Jen, *Chem. Mater.* **2010**, *22*, 2696.
[21] E. T. Hoke, K. Vandewal, J. A. Bartelt, W. R. Mateker, J. D. Douglas, R. Noriega, K. R. Graham, J. M. J. Fréchet, A. Salleo, M. D. McGehee, *Adv. Energy Mater.* DOI: 10.1002/aenm.201200474.
[22] B. A. Collins, J. R. Tumbleston, H. Ade, *J. Phys. Chem. Lett.* **2011**, *2*, 3135.
[23] W. Chen, T. Xu, F. He, W. Wang, C. Wang, J. Strzalka, Y. Liu, J. Wen, D. J. Miller, J. Chen, K. Hong, L. Yu, S. B. Darling, *Nano Lett.* **2011**, *11*, 3707.
[24] W. Yin, M. Dadmun, *ACS Nano* **2011**, *5*, 4756.
[25] F. C. Jamieson, E. B. Domingo, T. McCarthy-Ward, M. Heeney, N. Stingelin, J. R. Durrant, *Chem. Sci.* **2012**, *3*, 485.
[26] B. R. Aïch, J. Lu, S. Beaupré, M. Leclerc, Y. Tao, *Org. Electron.* **2012**, *13*, 1736.
[27] M. A. Faist, T. Kirchartz, W. Gong, R. S. Ashraf, I. McCulloch, J. C. de Mello, N. J. Ekins-Daukes, D. D. C. Bradley, J. Nelson, *J. Am. Chem. Soc.* **2012**, *134*, 685.
[28] J. C. Bijleveld, R. A. M. Verstrijden, M. M. Wienk, R. A. J. Janssen, *Appl. Phys. Lett.* **2010**, *97*, 073304.
[29] M. C. Scharber, D. Mühlbacher, M. Koppe, P. Denk, C. Waldauf, A. J. Heeger, C. J. Brabec, *Adv. Mater.* **2006**, *18*, 789.
[30] P. K. Nayak, G. Garcia-Belmonte, A. Kahn, J. Bisquert, D. Cahen, *Energy Environ. Sci.* **2012**, *5*, 6022.
[31] Z. M. Beiley, M. D. McGehee, *Energy Environ. Sci.* DOI: 10.1039/C2EE23073A.
[32] L. Dou, J. You, J. Yang, C. Chen, Y. He, S. Murase, T. Moriarty, K. Emery, G. Li, Y. Yang, *Nature Photon.* **2012**, *6*, 180.
[33] S. Cho, N. E. Coates, J. S. Moon, S. H. Park, A. Roy, S. Beaupré, D. Moses, M. Leclerc, K. Lee, A. J. Heeger, *Nature Photon.* **2009**, *3*, 297.
[34] N. C. Greenham, I. D. W. Samuel, G. R. Hayes, R. T. Phillips, A. B. Holmes, R. H. Friend, *Chem. Phys. Lett.* **1995**, *241*, 89.
[35] L. A. A. Pettersson, L. S. Roman, O. Inganäs, *J. Appl. Phys.* **1999**, *86*, 487.
[36] C. Melzer, E. J. Koop, V. D. Mihailetchi, P. W. M. Blom, *Adv. Funct. Mater.* **2004**, *14*, 865.
[37] W. Chen, M. P. Nikiforov, S. B. Darling, *Energy Environ. Sci.* **2012**, *5*, 8045.
[38] J. Rivnay, R. Steyrleuthner, L. H. Jimison, A. Casadei, Z. Chen, M. F. Toney, A. Facchetti, D. Neher, A. Salleo, *Macromolecules* **2011**, 5246.
[39] A. C. Mayer, M. F. Toney, S. R. Scully, J. Rivnay, C. J. Brabec, M. C. Scharber, M. Koppe, M. Heeney, I. McCulloch, M. D. McGehee, *Adv. Funct. Mater.* **2009**, *19*, 1173.
[40] E. Verploegen, R. Mondal, C. J. Bettinger, S. Sok, M. F. Toney, Z. Bao, *Adv. Funct. Mater.* **2010**, *20*, 3519.
[41] J. K. Lee, W. L. Ma, C. J. Brabec, J. D. Yuen, J. S. Moon, J. Y. Kim, K. Lee, G. C. Bazan, A. J. Heeger, *J. Am. Chem. Soc.* **2008**, *130*, 3619.
[42] D. R. Kozub, K. Vakhshouri, L. M. Orme, C. Wang, A. Hexemer, E. D. Gomez, *Macromolecules* **2011**, *44*, 5722.
[43] J. Rivnay, R. Noriega, R. J. Kline, A. Salleo, M. F. Toney, *Phys. Rev. B* **2011**, *84*, 1.
[44] A. M. Hindeleh, R. Hosemann, *J. Mater. Sci.* **1991**, *26*, 5127.
[45] H. Sirringhaus, P. J. Brown, R. H. Friend, M. M. Nielsen, K. Bechgaard, B. M. W. Langeveld-Voss, A. J. H. Spiering, R. A. J. Janssen, E. W. Meijer, P. Herwig, D. M. de Leeuw, *Nature* **1999**, *401*, 685.
[46] B. W. Boudouris, V. Ho, L. H. Jimison, M. F. Toney, A. Salleo, R. A. Segalman, *Macromolecules* **2011**, *44*, 6653.
[47] B. A. Collins, J. E. Cochran, H. Yan, E. Gann, C. Hub, R. Fink, C. Wang, T. Schuettfort, C. R. McNeill, M. L. Chabinyc, H. Ade, *Nat. Mater.* **2012**, *11*, 536.
[48] M. R. Hammond, R. J. Kline, A. A. Herzing, L. J. Richter, D. S. Germack, H.-W. Ro, C. L. Soles, D. A. Fischer, T. Xu, L. Yu, M. F. Toney, D. M. Delongchamp, *ACS Nano* **2011**, *5*, 8248.
[49] S. T. Turner, P. Pingel, R. Steyrleuthner, E. J. W. Crossland, S. Ludwigs, D. Neher, *Adv. Funct. Mater.* **2011**, *21*, 4640.
[50] B. A. Collins, E. Gann, L. Guignard, X. He, C. R. McNeill, H. Ade, *J. Phys. Chem. Lett.* **2010**, *1*, 3160.
[51] B. A. Collins, Z. Li, C. R. McNeill, H. Ade, *Macromolecules* **2011**, *44*, 9747.
[52] J. Y. Kim, C. D. Frisbie, *J. Phys. Chem. C* **2008**, *112*, 17726.
[53] B. A. Collins, Z. Li, J. R. Tumbleston, E. Gann, C. R. McNeill, H. Ade, *Adv. Energy Mater.* DOI: 10.1002/aenm.201200377.
[54] N. C. Cates, R. Gysel, Z. M. Beiley, C. E. Miller, M. F. Toney, M. Heeney, I. McCulloch, M. D. McGehee, *Nano Lett.* **2009**, *9*, 4153.
[55] G. F. Burkhard, E. T. Hoke, S. R. Scully, M. D. McGehee, *Nano Lett.* **2009**, *9*, 4037.
[56] J. L. Brédas, R. Silbey, D. S. Boudreaux, R. R. Chance, *J. Am. Chem. Soc.* **1983**, *371*, 6555.
[57] O. G. Reid, J. A. N. Malik, G. Latini, S. Dayal, N. Kopidakis, C. Silva, N. Stingelin, G. Rumbles, *J. Polym. Sci. Part B: Polym. Phys.* **2012**, *50*, 27.
[58] S. Bertho, G. Janssen, T. J. Cleij, B. Conings, W. Moons, A. Gadisa, J. D. Haen, E. Goovaerts, L. Lutsen, J. V. Manca, D. Vanderzande, *Sol. Energy Mater. Sol. Cells* **2008**, *92*, 753.
[59] J. Guo, Y. Liang, J. M. Szarko, B. Lee, H. J. Son, H. J. Son, B. S. Rolczynski, L. Yu, L. X. Chen, *J. Phys. Chem. B* **2010**, *114*, 742.
[60] A. L. Ayzner, D. D. Wanger, C. J. Tassone, S. H. Tolbert, B. J. Schwartz, *J. Phys. Chem. C* **2008**, *112*, 18711.
[61] B. A. Collins, H. Ade, *J. Electron Spectrosc. Relat. Phenom.* **2012**, *185*, 119.
[62] D. Chen, F. Liu, C. Wang, A. Nakahara, T. P. Russell, *Nano Lett.* **2011**, *11*, 2071.
[63] B. Watts, W. J. Belcher, L. Thomsen, H. Ade, P. C. Dastoor, *Macromolecules* **2009**, *42*, 8392.
[64] K. Vakhshouri, D. R. Kozub, C. Wang, A. Salleo, E. D. Gomez, *Phys. Rev. Lett.* **2012**, *108*, 026601.
[65] N. C. Cates, R. Gysel, J. E. P. Dahl, A. Sellinger, M. D. McGehee, *Chem. Mater.* **2010**, *22*, 3543.
[66] G. Griffini, J. D. Douglas, C. Piliego, T. W. Holcombe, S. Turri, J. M. J. Fréchet, J. L. Mynar, *Adv. Mater.* **2011**, *23*, 1660.
[67] I. R. Gearba, C.-Y. Nam, R. Pindak, C. T. Black, *Appl. Phys. Lett.* **2009**, *95*, 173307.
[68] G. F. Burkhard, E. T. Hoke, M. D. McGehee, *Adv. Mater.* **2010**, *22*, 3293.
[69] A. L. D. Kilcoyne, T. Tyliszczak, W. F. Steele, S. Fakra, P. Hitchcock, K. Franck, E. Anderson, B. Harteneck, E. G. Rightor, G. E. Mitchell, A. P. Hitchcock, L. Yang, T. Warwick, H. Ade, *J. Synchrotron Rad.* **2003**, *10*, 125.